Environ. Sci. Technol. **2004**, *38,* 2470−2475

Hydrate Composite Particles for Ocean Carbon Sequestration: Field Verification

COSTAS TSOURIS,*,† PETER BREWER,*,‡ EDWARD PELTZER,‡ PETER WALZ,‡ DAVID RIESTENBERG,† LIYUAN LIANG,† AND OLIVIA R. WEST†

Oak Ridge National Laboratory, P.O. Box 2008, Oak Ridge, Tennessee 37831-6181, and Monterey Bay Aquarium Research Institute, 7700 Sandholdt Road, Moss Landing, California 95039-9644

This paper reports on the formation and dissolution of CO_2/seawater/ CO_2 hydrate composite particles produced during field experiments in Monterey Bay, CA using a CO_2 injector system previously developed in the laboratory. The injector consisted of a coflow reactor wherein water was introduced as a jet into liquid CO_2, causing vigorous mixing of the two immiscible fluids to promote the formation of CO_2 hydrate that is stable at ambient pressures and temperatures typical of ocean depths greater than ∼500 m. Using flow rate ratios of water and CO_2 of 1:1 and 5:1, particulate composites of CO_2 hydrate/liquid CO_2/seawater phases were produced in seawater at depths between 1100 and 1300 m. The resultant composite particles were tracked by a remotely operated vehicle system as they freely traveled in an imaging box that had no bottom or top walls. Results from the field experiments were consistent with laboratory experiments, which were conducted in a 70 L high-pressure vessel to simulate the conditions in the ocean at intermediate depths. The particle velocity and volume histories were monitored and used to calculate the conversion of CO_2 into hydrate and its subsequent dissolution rate after release into the ocean. The dissolution rate of the composite particles was found to be higher than that reported for pure CO_2 droplets. However, when the rate was corrected to correspond to pure CO_2, the difference was very small. Results indicate that a higher conversion of liquid CO_2 to CO_2 hydrate is needed to form negatively buoyant particles in seawater when compared to freshwater, due primarily to the increased density of the liquid phase but also due to processes involving brine rejection during hydrate formation.

Introduction

The world's oceans are the primary natural sink for fossil fuel CO_2 released to the atmosphere (*1*). The net uptake of CO_2 is limited, however, primarily because of the slow ventilation rate or annual exposure of deep waters to the atmosphere (*2*). Injection of CO_2 into the oceans is being studied as a potential sequestration strategy for some fraction of the future production of fossil fuel CO_2 (*3*, *4*). Some 7 gt of C, released as anthropogenic CO_2, is currently produced per year (*1*). However, any ocean CO_2 injection scenario presents economic and environmental challenges (*5*, *6*). Lowering oceanic pH and increasing the CO_2 concentration near the injection point may present a biological impact (*7*−*10*). The economics of a deep injection must also be considered because deeper injection depths inevitably lead to increased injection energy penalties and costs. Finally, any method must minimize the potential for CO_2 to reenter the atmosphere. Sequestering CO_2 in the deep waters below the main oceanic thermocline (depths of >1000−1500 m) will result in extended residence times. The average ventilation age of deep ocean waters is approximately 250 years for the Atlantic and approximately 550 years for the Pacific (*11*).

Injection of CO_2 at depths >3500 m to form a CO_2 lake on the seafloor has been considered (*12*). Although this method will result in longer term sequestration, infrastructure and implementation costs increase significantly with greater injection depth, and the localized high concentration of CO_2 may cause negative biological effects. The identification of sites with suitable large-scale sea floor valleys close by a CO_2 source may also be difficult.

An alternative method is to release CO_2 as a positively buoyant plume of droplets (*13*, *14*). In this approach, the impact on benthic marine animals is minimized, and the release technology can be designed to minimize midwater impacts also. However, because of the rising nature of the plume, some of the work expended to carry out the injection is undone by the rise to shallower depths. The injection point must be sufficiently deep to allow complete dissolution of the liquid CO_2 into the surrounding seawater before the droplets reach depths at which the water masses are ventilated on short time scales (*15*).

Formation of a slowly dissolving negatively buoyant plume of CO_2 at intermediate depths is another way to address these challenges. In the case of a sinking plume, the goal of energy efficient deeper injection, and thus greater oceanic retention, is more easily met. Aya and co-workers (*16*) investigated the injection of cold liquid CO_2 and slurries of cold CO_2 with dry ice, which are denser than the surrounding seawater at intermediate depths. They observed that as cold CO_2 particles sink, ice forms on their surface, which lowers the density of the particles.

Another approach in producing dense CO_2 particles at intermediate depths is by promoting CO_2 hydrate formation. CO_2 hydrate is a nonstoichiometric solid phase of CO_2 and water that is thermodynamically stable at pressures equivalent to those typically found at >500 m depth (*12*), and pure CO_2 hydrate is approximately 10% denser than typical abyssal seawater (*17*). Therefore, complete conversion of CO_2 into hydrate would produce a negatively buoyant CO_2 phase at relatively shallow depths. Fully crystalline pure CO_2 hydrate is a hard solid, comparable to water ice; thus, it will not easily flow, and this presents severe problems for pipe disposal schemes. However, complete conversion of CO_2 to the hydrated phase is not necessary to create a negatively buoyant composite. For example, a composite slurry or paste consisting of water, liquid CO_2, and CO_2 hydrate will be negatively buoyant in seawater typically found at approximately 1000 m depth (*18*) with a 25% conversion of liquid CO_2 to hydrate. Such a composite also has the rheological characteristics required for flow. The hydrate also dissolves more slowly than liquid CO_2 (*19*−*21*), possibly lessening the local biological impacts of injection.

* Corresponding authors: (C.T.) e-mail: tsourisc@ornl.gov; phone: (865)241-3246; fax: (865)241-4829; (P.B.) e-mail: brpe@mbari.org; phone: (831)775-1706; fax: (831)775-1645.

† Oak Ridge National Laboratory.

‡ Monterey Bay Aquarium Research Institute.

10.1021/es034990a CCC: $27.50 © 2004 American Chemical Society
Published on Web 03/13/2004

A method was recently developed to partially convert a stream of liquid-phase CO_2 to CO_2 hydrate using a CO_2/water coflow jet reactor (*18*, *22*). In the reactor, water was introduced as a jet and vigorously mixed into liquid CO_2, continuously forming a composite paste of liquid CO_2, CO_2 hydrate, and water. In experiments with seawater, dense brine resulting from salt rejection during hydrate formation is also included. The composite paste, deformable enough to flow, but dense enough to at least equal the surrounding fluid, was extruded from the reactor into the surrounding water. Experiments were previously performed in the laboratory to determine the flow rates of CO_2 and water in the reactor necessary for the formation of a negatively buoyant composite at pressures of 10−13 MPa (approximately equivalent to 1−1.3 km ocean depth) (*23*).

This paper reports the results of field injection experiments that were performed in Monterey Bay, CA at 1100−1300 m depth using the same coflow jet reactor and varying flow rates of CO_2 and water. The velocity and changing dimensions of the composite cylindrical slugs extruded were determined by using a highly instrumented remotely operated vehicle (ROV) (*15*) to track the particles as they traveled through the water column. The density and composition of the particles were calculated, as was the composite dissolution rate. The results are compared with those obtained in the laboratory.

Materials and Methods

Coflow Jet Reactor. The coflow jet reactor (Figure 1A) has been developed and used to extrude a composite paste of liquid CO_2/water/CO_2 hydrate in the laboratory (*18*, *23*). The reactor consisted of an outer tube (o.d. of 9.5×10^{-3} m and i.d. of 6.4×10^{-3} m) and a concentrically located inner capillary tube (o.d. of 1.6×10^{-3} m and i.d. of 0.254×10^{-3} m). This design permits spraying of water droplets through the capillary tube into liquid CO_2 that is continuously pumped in the reactor via the outer tube. The stainless steel capillary tube terminated approximately 0.14 m from the end of the outer tube, creating a zone in which the liquid CO_2 and water could vigorously mix, enhancing the production of CO_2 hydrate. The outer tube consists primarily of stainless steel with a 0.125 m section of Teflon at the end; this construction prevents wetting of the wall by the water phase in the mixing zone and keeps water finely dispersed in the CO_2 liquid phase. The composite particles are produced in the mixing zone before being discharged into the ambient water. In laboratory experiments using a 72 L pressure vessel (description in ref *22*), water and liquid CO_2 were delivered through the inner capillary and outer tubes via syringe pumps at predetermined flow rates of 15−25 and 2−10 mL/min, respectively. In previous laboratory studies, water droplets produced via the capillary averaged 267 ± 79 μm (*23*).

Field Experiments. The coflow jet reactor was field tested in ocean waters from 1100 to 1300 m in depth in Monterey Bay, CA. The ROV *Ventana* was deployed by the RV *Point Lobos* to perform the injections. The injector was mounted in a Plexiglas box (0.3 m wide, 0.25 m deep, and 0.91 m high) that was open at the top and bottom (Figure 1B) and had an illuminated translucent rear panel. A picture of the ROV *Ventana* carrying the injector inside the Plexiglass box is presented in Figure 2. The box allowed the injected composite particles to rise or fall freely based on their buoyancy but restricted lateral motion (*15*), thus easing the vehicle piloting requirements. The illuminated rear wall of the box served to back light the particles and also to screen out visual clutter from the ubiquitous midwater animals and marine snow. Carbon dioxide and ambient seawater were pumped via a piston assembly, as described earlier (*24*). Volumetric flow meters were installed to measure the flow rates of the fluids as they were introduced into the coflow jet reactor and were arranged so that they were viewable with the primary HDTV camera system. Injections were performed using a 1:1 volumetric ratio of CO_2 to water at ~1000 m depth to produce a floating composite and with a 1:5 ratio at ~1300 m depth to produce a sinking composite. The size and velocity of the resultant particles were determined using the ROV, which traveled vertically to follow one randomly selected particle for each injection experiment through the water column and recorded the particle using a HDTV camera as described previously (*15*). Selected video frames in which the particle appeared to be oriented parallel to the front Plexiglas plane were processed post cruise, using image analysis software (*Scion Image*) to determine the dimensions of the particle. Scales on the front and rear planes of the Plexiglas imaging box were used to measure the length and diameter of the cylindrical composite particles. To correct for errors introduced by the 0.25 m depth of the imaged field, the dimensions of the composite particles were taken as the average of the dimensions based on the front and rear calibration scales.

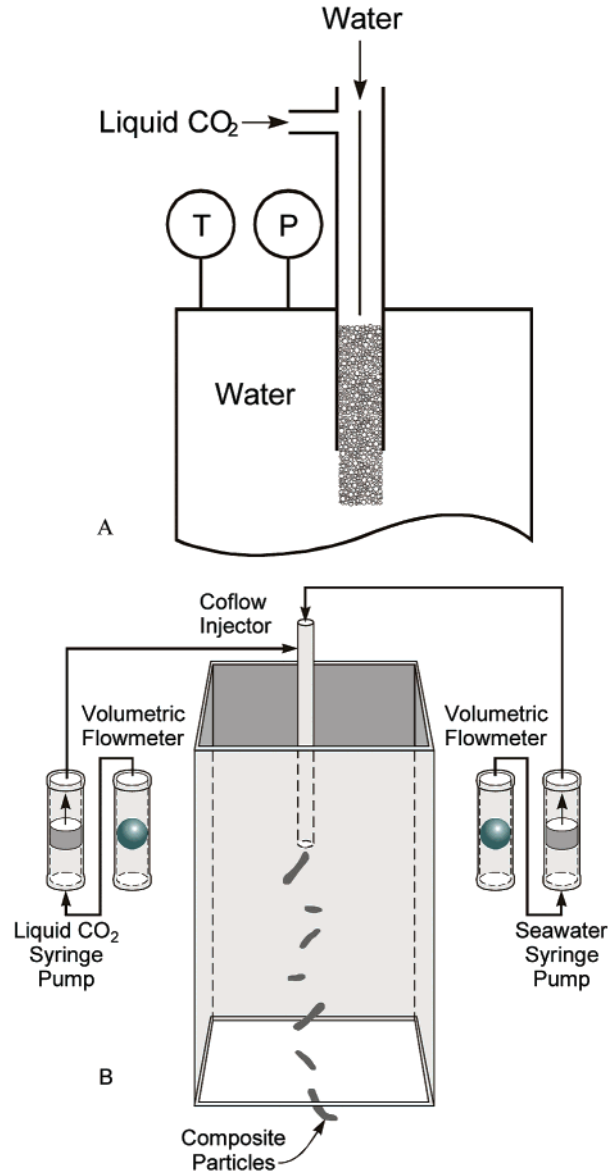

FIGURE 1. Schematics showing (A) laboratory design for injection of liquid CO_2 and water using a coflow jet reactor and (B) coflow jet reactor, syringe pumps, and flowmeters used for ocean injections of composite particles performed at 1000−1300 m ocean depth on the ROV *Ventana*. The Plexiglas box was open at the top and bottom, allowing the composite to freely rise or sink after injection.

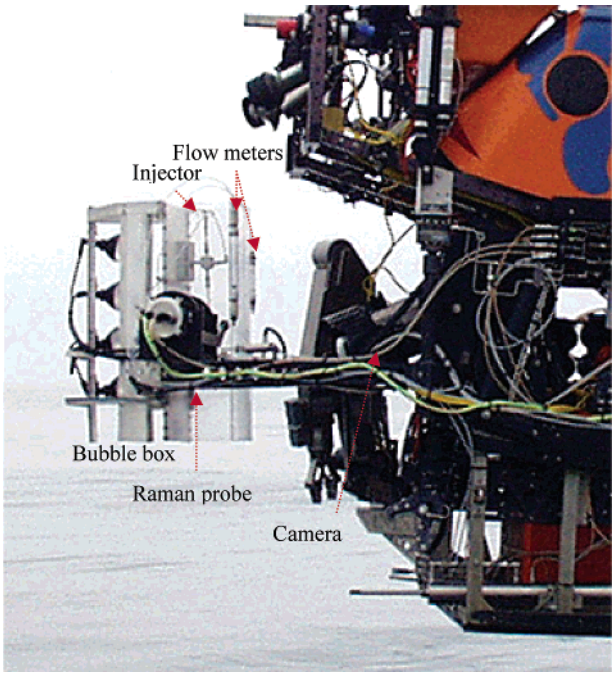

FIGURE 2. ROV *Ventana* carrying the experimental apparatus about to enter the water. The front of the imaging box faces toward the vehicle. The lights arranged to illuminate the rear translucent screen are at the far left, the flow meters are on the box front corners, and the coflow reactor is mounted on the rear wall. The CO_2 cylinder and water pump are mounted under the vehicle and connected by tubing to the valves mounted on the box. See Figure 1B for a more detailed schematic of the Plexiglass box.

The seawater depth, temperature, density, and pressure were logged using the instrumentation suite installed on the ROV, and recorded in time sequence throughout the experiment from the production of the composite particles through their dissolution. These data were then used to estimate particle velocity, density, and dissolution rate.

Results

Description of Field Injection. Liquid CO_2/water/CO_2 hydrate composite particles were successfully created during field injections in Monterey Bay, CA at ocean depths of 1100−1300 m. The composite produced in the field (Figure 3B) was similar in appearance to that produced in previous laboratory experiments (Figure 3A) at equivalent pressures and temperatures in a 3.5% NaCl solution. The diameters of both the laboratory- and field-produced composites are approximately 6.5 mm. Data from the field experiments showed that the resultant composite particles varied from 5 to 85 mm in length, with an average of length 29 ± 18 mm. The particles were observed to shrink in diameter and length over time in the ambient seawater. The direction and velocity of their motion depended on the injection depth (or pressure), as well as the ratio of CO_2 to water injected. Figure 4 shows the vertical path of three particles through the water column from three different injection runs. There were mild currents during and after injections, which may have effected the instantaneous measurements of particle velocity; however, the effect over their entire travel time was insignificant. Particles appeared to become more positively buoyant over time (Figure 4) due to dissociation of hydrate.

In the first injection experiment, run number 163−1107, composite particles were successfully produced using flow rates of 50 mL/min for both seawater and CO_2, respectively, in the coflow jet reactor. The injection was performed at a depth of 1099.4 m where the temperature was 3.57 °C. The injected composite was followed by the ROV as it rose vertically to a depth of 1061.8 m (37.5 m from the release point) over a period of 10 min and 20 s (Figure 4), where the temperature was 3.69 °C. After that point, the composite became too small to follow. The positive buoyancy of these composite particles was expected based on our previous laboratory studies (*23*), which showed that a flow rate ratio for CO_2/H_2O of less than 1:3 is needed to form a negatively buoyant composite.

Two subsequent injections were performed, run numbers 164−1226 and 164−1232, in which attempts were made to produce a sinking composite. These injections were performed at a greater depth than run 163−1107 (the floating experiment). With increasing depth, the density of the highly compressible liquid CO_2 increases faster than that of the incompressible seawater, contributing to the net density contrast of the composite particles created (*14*). The water flow rate was maintained at 50 mL/min, but the CO_2 flow rate was reduced to 10 mL/min to give a 1:5 ratio for CO_2/H_2O in the injector.

Injection run 164−1226 was performed at a depth of 1251 m and temperature of 3.68 °C. A resultant composite particle

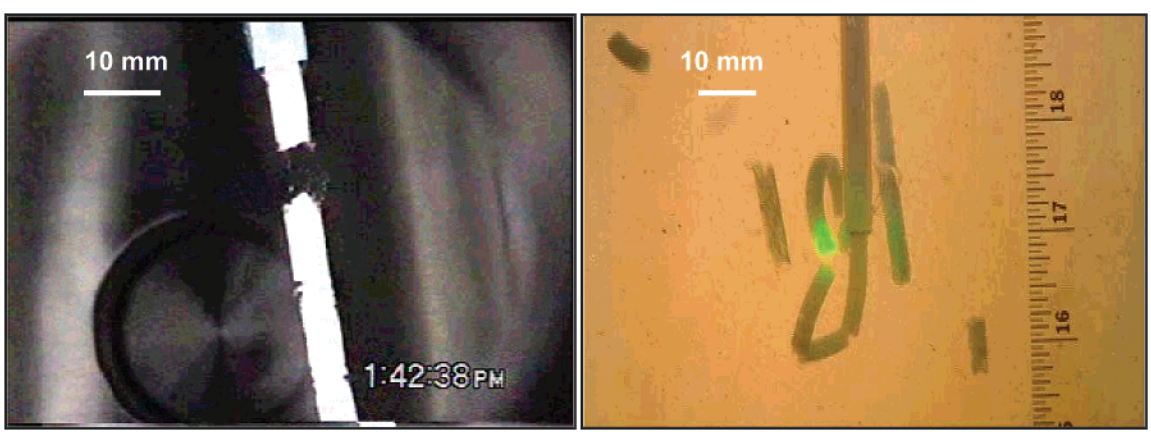

A B

FIGURE 3. Microphotographs of (A) laboratory and (B) ocean injections of CO_2 hydrate. (A) CO_2 hydrate injection in the Oak Ridge National Laboratory Seafloor Process Simulator using the coflow jet reactor at $P = 10.5$ MPa and $T = 4.1$ °C. Flow rates for water and CO_2 were 25 and 6 mL/min, respectively. (B) CO_2 hydrate injection in Monterey Bay, CA, using the coflow jet reactor at 1290 m depth ($P = 13.1$ MPa and $T = 3.2$ °C). Flow rates for water and CO_2 were 50 and 10 mL/min, respectively. Note: The light on one of the particles in the field experiment comes from a Raman spectrometer that was unsuccessfully used to analyze composite particles.

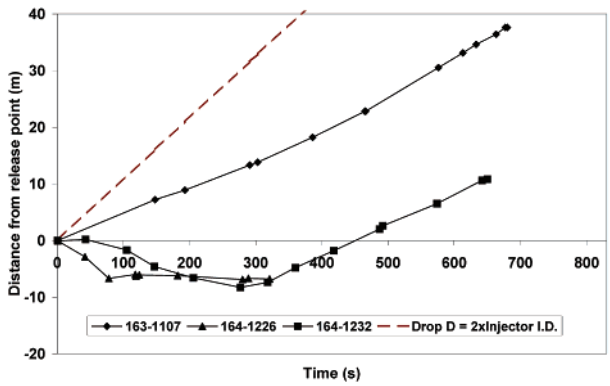

FIGURE 4. Plot of particle depth vs time, indicating the vertical movement of particles after injection. Predicted path of liquid CO_2 droplet released at same depth as 163−1107 with a diameter twice that of the injector is also shown.

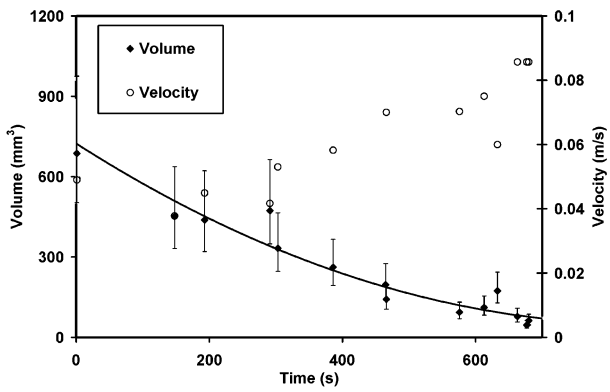

FIGURE 5. Volume and velocity histories of a particle after the 163−1107 injection at 1090 m depth.

was followed for 5 min and 21 s during which time it initially sank slowly and then became neutrally buoyant at a depth of 1258 m (6.8 m below the release point) and a temperature of 3.26 °C (Figure 4). Injection run 164−1232 was performed at a depth of 1297 m and a temperature of 3.24 °C. A composite particle was followed for 10 min and 46 s during which time it initially moved slowly downward and then floated to a depth of 1286 m (11 m above the release point); the particle was then too small to be followed and imaged by the ROV (Figure 4). A CO_2 droplet is expected to rise at roughly twice the velocity (*15*) of the particle in run 163−1107, assuming a drop diameter of 1.28 cm (twice the diameter of the injector) and neglecting the effect of any CO_2 conversion to hydrate on the surface of the droplet. This layer remains relatively thin ($\sim 10^{-5}$ m) based on previous experiments (*25*). This illustrates the benefits of premixing water into the CO_2 stream to promote hydrate formation prior to injection; CO_2 ocean sequestration techniques can thus be improved even for positively buoyant particles.

The length and diameter of one randomly selected composite particle for each injection experiment were measured as they moved through the water column. In all cases, the particles were observed to decrease in length and diameter over time. The uncertainty in the location of the particles within the imaging depth of field likely resulted in errors when measuring the particle dimensions. Figure 5 shows the volume and velocity of the particle followed in injection run 163−1107 over time, with error bars to show the maximum and minimum possible volume based on the rear and front scales, respectively. Similar calculations were made for the other injection runs (not shown).

Analysis of Injections. For each experiment, the particle density (ρ_p) was estimated from the particle dimensions and velocity using the following equation:

$$\rho_p = \rho_w + i\frac{3C_D\rho_w U_p^{\,2}}{4D_{ps}g} \tag{1}$$

obtained from the balance of buoyancy and drag forces on a spherical particle having the same volume as the cylindrical particle (*26*). In eq 1, C_D is the drag coefficient, ρ_w is the density of seawater at the injection depth, U_p is the vertical velocity of the particle, i is +1 for a sinking particle and −1 for a floating particle, g is the gravity constant, and D_{ps} is the diameter of the equivalent spherical particle $(1.5D_{pc}^2L_p)^{1/3}$, where L_p is the particle length and D_{pc} is the particle diameter. The length, diameter, and velocity for each particle immediately after it was released from the injector were used for calculating the particle densities.

The drag coefficient in eq 1 was obtained from a published correlation between C_D and Reynolds number (R_e) (*26*). The Reynolds number of the equivalent spherical particle is defined as

$$R_e = \frac{D_{ps}U_p\rho_w}{\mu_w} \tag{2}$$

where μ_w is the seawater viscosity (0.014 g/cm s). The Reynolds number was determined for each particle and was found to be approximately 490, 180, and 0 for particles 163−1107, 164−1226, and 164−1232, respectively, using the particle velocity just after injection. For the sake of simplicity, the particles are considered spherical in estimating the drag coefficient (C_D). For a Reynolds number range of 1−1000, the relationship of R_e to C_D for a sphere has been established as (*26*)

$$C_D \cong \frac{18.5}{R_e^{\,3/5}} \tag{3}$$

The calculated drag coefficients for the particles were 0.45 and 0.81 for particles in runs 163−1107 and 164−1226. The particle in run 164−1232 had zero vertical velocity, in which case a drag coefficient does not apply.

The hydrate conversion factor, x_h, in the particles tracked under each experiment can be calculated from the estimated density of the composite particles. The density is also a function of the hydrate density ρ_h, CO_2 and water densities, the moles of CO_2 and water initially present in the composite particle (i.e., before hydrate formation) n_c and n_w, and the hydration number n (*23*):

$$\rho_p = \frac{44n_c + 18n_w}{44n_c(1/\rho_c - x_h(1/\rho_c - 1/\rho_h)) - 18(nx_h n_c(1/\rho_w - 1/\rho_h) - n_w/\rho_w} \tag{4}$$

For a given volumetric flow rate ratio between CO_2 and water, λ, the ratio between n_c and n_w is as follows:

$$\frac{n_c}{n_w} = \frac{18\rho_c\lambda}{44\rho_w} \tag{5}$$

Substituting eq 5 into eq 4 and rearranging, the hydrate conversion x_h can be calculated from the flow rate ratio λ, the composite density ρ_p estimated from eq 1, and phase densities

$$x_h = \frac{(1/\rho_c - 1/\rho_p) + (\rho_w/\rho_c)(1/\lambda)(1/\rho_w - 1/\rho_p)}{(1/\rho_c - 1/\rho_h) + 18n(1/\rho_w - 1/\rho_h)/44} \tag{6}$$

The estimated hydrate conversion for each injection experi-

TABLE 1. Summary of Field Data and Calculated Results from Three Injections

	experiment no.		
	163−1107	164−1226	164−1232
observed initial behavior	floating	sinking	neutral
injection depth (m)	1099	1251	1297
phase densities (kg/m^3): CO_2 liquid	943	955	957
Seawater	1032.60	1033.31	1033.53
CO_2 hydrate	1100	1100	1100
particle velocity (m/s)	−0.06	+0.02	0
initial particle length (mm)	24.6	34	26.2
initial particle diameter (mm)	6.0	6.1	5.7
initial volume of composite (10^{-6} m^3)	0.687	0.986	0.692
estimated composite density (kg/m^3)	1020.9	1035.4	1033.5
volumetric flow rate ratio (Q_{CO_2}/Q_W)	1	0.2	0.2
CO_2 hydrate conversion (x_h)	0.21	0.30	0.26
minimum conversion for sinking composite ($x_{h\ min}$)	0.2864	0.2593	0.2551

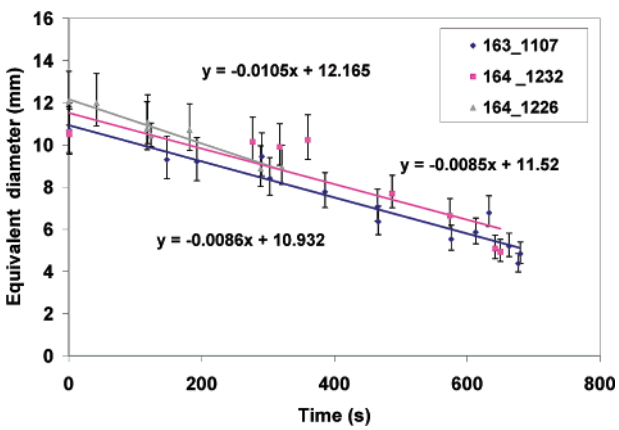

FIGURE 6. Dissolution of composite particles.

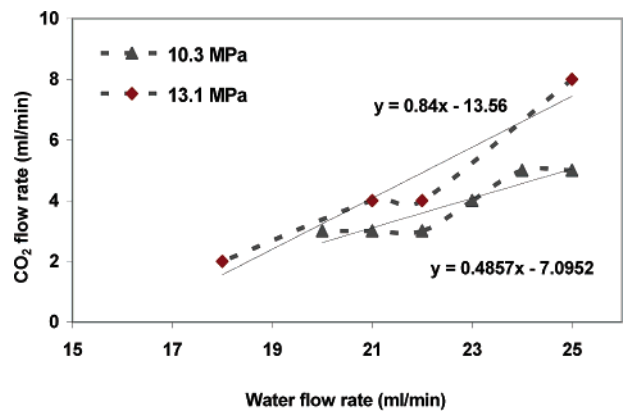

FIGURE 7. Flow rate limits of CO_2 and simulated seawater (3.5% NaCl aqueous solution) necessary for producing negatively buoyant composite particles in the Seafloor Process Simulator. Experiments were conducted with the vessel filled with a 3.5% NaCl solution. Composite produced using flow rates of CO_2 and NaCl solution above the line were positively buoyant, while those below the line sank.

ment is shown in Table 1 and compared with the minimum CO_2 hydrate conversion necessary to produce a neutrally buoyant particle $x_{h\ min}$ (where $\rho_p = \rho_w$ in eq 4) for a particular depth (*23*):

$$x_{h\ min} = \frac{1/\rho_c - 1/\rho_w}{(1/\rho_c - 1/\rho_h) + 18n(1/\rho_w - 1/\rho_h)/44} \quad (7)$$

Consistent with previous laboratory experiments, the hydrate conversion in 163−1107 is lower than in the other experiments due to a higher flow rate ratio between CO_2 and water.

The rate of particle shrinkage over time allows a comparison of the dissolution rates of composite particles with those observed for hydrate-covered CO_2 droplets by others. Figure 6 shows the equivalent spherical diameter D_{ps} for each particle after injection as a function of time. The overall particle shrinkage rates calculated for the injection runs 164−1226 and 164−1232 were 10.5×10^{-6} and 8.5×10^{-6} m/s, respectively, while that for injection run 163−1107 was 8.6×10^{-6} m/s. The error in the dissolution rates was calculated based on the error in the measurement of the dimensions of the particles and was approximately $\pm 1 \times 10^{-6}$ m/s. Radhakrishnan et al. (*21*) recently reviewed the dissolution rates of hydrate-covered CO_2 droplets and reported them to range between 10^{-6} and 10^{-8} m/s. Brewer et al. (*15*) recently performed injections of CO_2 droplets at 800 m depth in Monterey Bay and reported a dissolution rate of approximately 3×10^{-6} m/s. The composite particles investigated in this work appear to have a higher shrinkage rate than those observed for droplets covered with hydrate. Because the composite particles contain considerable amounts of water, it is reasonable to correct for the presence of water to convert the shrinkage rate to an equivalent CO_2 dissolution rate. If we assume that the CO_2 fraction is less than 1/3 of the initial mixture, then the dissolution rate corresponding to pure CO_2 averaged between 3×10^{-6} and 3.5×10^{-6} m/s, which is similar to the values reported by Brewer and co-workers (*15*).

Comparison of Field and Laboratory Data. Laboratory experiments were conducted with the coflow jet reactor prior to ocean injections (*18, 23*). The results of those injections showed that for a given water flow rate, there was a maximum CO_2 flow rate above which a floating composite was produced and below which sinking composite was produced (Figure 7). From the laboratory results, it is apparent that as the water flow rate increased more CO_2 could be injected while the composite remained negatively buoyant. Because of pump limitations, the maximum water flow rate available for the laboratory injections was 25 mL/min. Because the water flow rate in the ocean injections was limited to 50 mL/min, a direct comparison cannot be made. However, if the laboratory results are extrapolated to higher water flow rates, the maximum flow rate of CO_2 per nozzle of this design that will produce a sinking composite with 50 mL/min water would be 17.2 mL/min at 10.3 MPa and 28.4 mL/min at 13.1 MPa (using linear extrapolation in Figure 7). Injection run 163−1107 was performed at 10.99 MPa with a CO_2 flow rate of 50 mL/min. These conditions produced a floating particle composite and lower hydrate conversion as predicted by the laboratory flow rate ratios. Injection runs 164−1226 and 164−

1232, however, were performed with a CO_2 flow rate of 10 mL/min, which, according to the laboratory experiment, should give a negatively buoyant composite. Instead, the particles were neutrally buoyant. This result suggests a nonlinear behavior, which should be expected because of the complexity of the system and the dependency on mixing conditions. In terms of the capillary Reynolds number, in the laboratory experiments this parameter varied between 2200 and 2900, which is close to the transitional region from laminar to turbulent flow. In the field injections, however, the capillary R_e was approximately 5900, which is in the turbulent regime. Further laboratory studies on composites produced by using higher flow rates are planned.

In conclusion, solid CO_2/water/CO_2 hydrate composite paste-like particles were successfully formed and extruded in ocean injections at depths of 1100−1300 m using a coflow CO_2/water injector. Particles were tracked vertically after injection and were found to be either slightly positively buoyant or neutral, depending on the amount of CO_2 injected and the injection depth. Conversion of CO_2 to hydrate in the composite ranged from 21 to 30%. Future challenges include modifying the injection system to increase conversion and produce a slowly dissolving, negatively buoyant CO_2 phase that can be used for ocean carbon sequestration.

Acknowledgments

Gratefully acknowledged is support by the Ocean Carbon Sequestration Program, Office of Biological and Environmental Research, U.S. Department of Energy, Grant KP120203, under Contract DE-AC05-00OR22725 with UT-Battelle, LLC. Support for MBARI was provided by the David and Lucile Packard Foundation and by the U.S. Department of Energy under Contracts DE-FC26-00NT40929 and DE-FG03-01-ER63065. We thank the captain and crew of the RV *Point Lobos* and the pilots of the ROV *Ventana* for making the field experiments possible and Dr. Marsha Savage for editing the manuscript.

Literature Cited

(1) *Intergovernmental Panel on Climate Change: The Science of Climate Change*; Cambridge University Press: New York, 1995; p 572.
(2) McNeil, B.; Matear, R. J.; Key, R. M.; Bullister, J. L.; Sarmiento, J. L. *Science* **2003**, *299*, 235−239.
(3) Medina, M.-G.; Bond, G. M.; Stringer, J. *Interface* **2001**, *10* (1), 26−30.
(4) Hoffert, M. I.; Caldeira, K.; Benford, G.; Criswell, D. R.; Green, C.; Herzog, H.; Jain, A. K.; Kheshgi, H. S.; Lackner, K. S.; Lewis, J. S.; Lightfoot, H. D.; Manheimer, W.; Mankins, J. C.; Mauel, M. E.; Perkins, L. J.; Schlesinger, M. E.; Volk, T.; Wigley, T. M. L. *Science* **2002**, *298*, 981−987.
(5) Golomb, D. *Energy Convers. Manage.* **1993**, *34*, 967−976.
(6) Adams, E. E.; Golomb, D. S.; Herzog, H. J. *Energy Convers. Manage.* **1995**, *36*, 447−452.
(7) Auerbach, D. I.; Caulfield, J. A.; Adams E. E.; Herzog, H. J. *Environ. Model. Assess.* **1997**, 333−343.
(8) Tamburri, M. N.; Peltzer, E. T.; Friederich, G. E.; Aya, I.; Yamane, K.; Brewer, P. G. *Mar. Chem.* **2000**, *72*, 95−101.
(9) Takeuchi, K.; Fujioka, Y.; Kawasaki, Y.; Shirayama, Y. *Energy Convers. Manage.* **1997**, *38*, 5337−5341.
(10) Seibel, B. A.; Walsh P. J. *Science* **2001**, *294*, 379−380.
(11) Stuiver, M.; Quay, P. D.; Ostlund, H. G. *Science* **1983**, *219*, 849−851.
(12) Brewer, P. G.; Friederich, G.; Peltzer, E. T.; Orr, F. M., Jr. *Science* **1999**, *284*, 943−945.
(13) Liro, C. R.; Adams, E. E.; Herzog, H. G. *Energy Convers. Manage.* **1992**, *33*, 667−674.
(14) Alendal, G.; Drange, H. *J. Geophys. Res.* **2001**, *106*, 1085−1096.
(15) Brewer, P. G.; Peltzer, E. T.; Friederich, G.; Rehder, G. *Environ. Sci. Technol.* **2002**, *36*, 5441−5446.
(16) Aya, I.; Kojima, R.; Yamane, K.; Shiozaki, K.; Brewer, P. G.; Peltzer, E. T., III. *Energy*, in press.
(17) Sloan, E. D., Jr. *Clathrate Hydrates of Natural Gases*, 2nd ed.; Marcel Dekker: New York, 1998.
(18) West, O. R.; Tsouris, C.; Liang, L.; Lee, S.-Y.; McCallum, S. D. *AIChE J.* **2003**, *49*, 283−285.
(19) Aya, I.; Yamane, K.; Nariai, H. *Energy* **1997**, *22*, 263−271.
(20) Hirai, S.; Okazaki, K.; Tabe, Y.; Hijikata, K.; Mori, Y. *Energy* **1997**, *22*, 285−293.
(21) Radhakrishnan, R.; Demorov, A.; Herzog, H.; Trout, B. L. *Energy Convers. Manage.* **2003**, *44*, 773−782.
(22) Phelps, T. J.; Peters, D. J.; Marshall, S. L.; West, O. R.; Liang, L.; Blencoe, J. G.; Alexiades, V.; Jacobs, G. K.; Naney, M. T.; Heck, J. L., Jr. *Rev. Sci. Instrum.* **2001**, *72*, 1514−1521.
(23) Lee, S.-Y.; Liang, L.; Riestenberg, D. E.; West, O. R.; Tsouris, C.; Adams, E. E. *Environ. Sci. Technol.* **2003**, *37*, 3701−3708.
(24) Brewer, P. G.; Orr, F. M., Jr.; Friederich, G.; Kvenvolden, K. A.; Orange, D. *Energy Fuels* **1998**, *12*, 183−188.
(25) Teng, H.; Yamasaki, A.; Shindo, Y. *Chem. Eng. Sci.* **1996**, *51*, 4979−4986.
(26) Tek, M. R.; Wilkes, J. O. *Fluid Flow and Heat Transfer*; University of Michigan: Ann Arbor, 1974.

Received for review September 8, 2003. Revised manuscript received January 27, 2004. Accepted February 3, 2004.

ES034990A